AMERICAN SOCIETY FOR MICROBIOLOGY | Journal of Virology®

VIRUS-CELL INTERACTIONS

Antiapoptotic Clone 11-Derived Peptides Induce *In Vitro* Death of CD4$^+$ T Cells Susceptible to HIV-1 Infection

Anastassia Mikhailova,[a,d] José Carlos Valle-Casuso,[a] Annie David,[a] Valérie Monceaux,[a] Stevenn Volant,[b] Caroline Passaes,[a] Amal Elfidha,[a,e] Michaela Müller-Trutwin,[a] Jean-Luc Poyet,[c] Asier Sáez-Cirión[a]

[a]Institut Pasteur, Unité HIV Inflammation et Persistance, Paris, France
[b]Institut Pasteur, Hub Bioinformatique et Biostatistique, C3BI, USR 3756 IP CNRS, Paris, France
[c]INSERM UMRS976, Institut de Recherche Saint Louis, Hôpital Saint Louis, Paris, France
[d]Université Paris Diderot, Université de Paris, Paris, France
[e]Université Paris Descartes, Université de Paris, Paris, France

ABSTRACT HIV-1 successfully establishes long-term infection in its target cells despite viral cytotoxic effects. We have recently shown that cell metabolism is an important factor driving CD4$^+$ T cell susceptibility to HIV-1 and the survival of infected cells. We show here that expression of antiapoptotic clone 11 (AAC-11), an antiapoptotic factor upregulated in many cancers, increased with progressive CD4$^+$ T cell memory differentiation in association with the expression of cell cycle, activation, and metabolism genes and was correlated with susceptibility to HIV-1 infection. Synthetic peptides based on the LZ domain sequence of AAC-11, responsible for its interaction with molecular partners, were previously shown to be cytotoxic to cancer cells. Here, we observed that these peptides also blocked HIV-1 infection by inducing the death of HIV-1-susceptible primary CD4$^+$ T cells across all T cell subsets. The peptides targeted metabolically active cells and had the greatest effect on effector and transitional CD4$^+$ T cell memory subsets. Our results suggest that the AAC-11 survival pathway is potentially involved in the survival of HIV-1-infectible cells and provide proof of principle that some cellular characteristics can be targeted to eliminate the cells offering the best conditions to sustain HIV-1 replication.

IMPORTANCE Although antiretroviral treatment efficiently blocks HIV multiplication, it cannot eliminate cells already carrying integrated proviruses. In the search for an HIV cure, the identification of new potential targets to selectively eliminate infected cells is of the outmost importance. We show here that peptides derived from antiapoptotic clone 11 (AAC-11), whose expression levels correlated with susceptibility to HIV-1 infection of CD4$^+$ T cells, induced cytotoxicity in CD4$^+$ T cells showing the highest levels of activation and metabolic activity, conditions known to favor HIV-1 infection. Accordingly, CD4$^+$ T cells that survived the cytotoxic action of the AAC-11 peptides were resistant to HIV-1 replication. Our results identify a new potential molecular pathway to target HIV-1 infection.

KEYWORDS AAC-11, CD4 T cells, apoptosis, cell metabolism, human immunodeficiency virus, susceptibility to infection

Human immunodeficiency virus type 1 (HIV-1) disease is a persistent viral infection that has claimed millions of lives around the globe. The era of combination antiretroviral therapy (cART) has extended the life expectancy of people living with HIV and improved their quality of life. However, although cART blocks viral replication, it does not eliminate infected cells, which persist despite decades of treatment and originate viral rebound if therapy is interrupted (1–3). There is, therefore, a need to identify characteristics of HIV-infected cells that could be potentially targeted by new

Citation Mikhailova A, Valle-Casuso JC, David A, Monceaux V, Volant S, Passaes C, Elfidha A, Müller-Trutwin M, Poyet J-L, Sáez-Cirión A. 2020. Antiapoptotic clone 11-derived peptides induce *in vitro* death of CD4$^+$ T cells susceptible to HIV-1 infection. J Virol 94:e00611-20. https://doi.org/10.1128/JVI.00611-20.

Editor Frank Kirchhoff, Ulm University Medical Center

Address correspondence to Asier Sáez-Cirión, asier.saez-cirion@pasteur.fr.

Received 6 April 2020
Accepted 23 April 2020
Accepted manuscript posted online 29 April 2020
Published 1 July 2020

therapeutic strategies. CD4$^+$ T cells are primary targets of HIV-1, but the cells differ in their relative susceptibility to infection (4–6). HIV requires a particular cell environment providing abundant factors that the virus exploits to sustain its replication cycle. Susceptibility to HIV infection *in vitro* increases with CD4$^+$ T cell differentiation. Naive CD4$^+$ T cells are most resistant, while central memory (Cm), transitional memory (Tm), and effector memory (Em) CD4$^+$ T cells are progressively more susceptible to the virus. We have recently shown that these differences are, at least in part, related to the increased metabolic activity associated with progressive differentiation of these subsets (7). Immunometabolism is a critical element in the regulation of T cell differentiation, survival, and function (8). Upon antigenic stimulation, T cells upregulate metabolic fluxes to provide the energy necessary to support cellular processes and to increase the pool of substrates necessary for building proteins, lipids, nucleic acids, and carbohydrates. This metabolically rich environment is necessary for the establishment of both productive and latent HIV infections (7, 9, 10), as is also the case for other infections (11–13), and may offer new opportunities to tackle HIV.

In a *post hoc* analysis of results obtained in our previous study (7), we found that antiapoptotic clone 11 (AAC-11) (also known as apoptosis inhibitor 5 [API5]) was significantly correlated with infection in different subsets of memory CD4$^+$ T cells. The antiapoptotic activity of AAC-11 might contribute to the survival of metabolically active cells. Indeed, AAC-11 is overexpressed in many cancers (14) and allows cancer cell survival under conditions of metabolic stress (15). Its expression is associated with poor prognosis in non-small cell lung and cervical cancers (16–18). Although the mechanisms associated with its antiapoptotic activity have not been clearly elucidated, AAC-11 contains several protein interaction domains, including a leucine zipper (LZ) domain (19), and has been proposed to repress apoptotic effectors, such as E2F1 (20), Acinus (21), and caspase 2 (22). Synthetic peptides based on the LZ domain sequence of AAC-11 were previously shown to be cytotoxic to cancer cells both *in vitro* and in an *in vivo* mouse model of melanoma (23, 24) or acute leukemia (25).

We explore here whether AAC-11-derived peptides could, similarly to its action against cancer cells, induce the elimination of HIV-1-infected cells. We found that AAC-11-derived peptides were preferentially cytotoxic for CD4$^+$ T cells targeted by HIV-1. In contrast, cells escaping the cytotoxic action of the peptides were resistant to HIV-1 replication. These results offer proof of principle that some characteristics of the cells targeted by the virus could be antagonized to counteract infection.

RESULTS

AAC-11-derived peptides display antiviral activity against diverse HIV-1 strains and simian immunodeficiency virus (SIV). We previously analyzed the susceptibility of memory CD4$^+$ T cell subpopulations (Cm, Tm, and Em cells) to HIV-1 infection (7). We also analyzed the expression, at the time of infection, of a panel of 96 genes related to T cell differentiation, function, and survival, as well as restriction and HIV-facilitating factors (https://data.mendeley.com/datasets/vfj3r27gnf/1). Among other genes, we found in *post hoc* analysis that the expression of antiapoptotic factor AAC-11 increased progressively with the stage of differentiation of memory CD4$^+$ T cells (Cm $<$ Tm $<$ Em) and was correlated with infection in these subsets (Fig. 1a and b). The expression of AAC-11 was strongly correlated with the expression of multiple genes related to cell metabolism (e.g., SLC1A5, MTOR, HIF1A, GUSB, and GAPDH [glyceraldehyde-3-phosphate dehydrogenase] genes) and the cell cycle (e.g., RHOA, RB1, MAPK1, and MKI67 genes) and genes known to be necessary for different steps of the HIV replication cycle (RRM2, SAMRCB1, DDB1, CFL1, ACTB, CDK9, and NFKB1 genes) (26–42) (Fig. 1c). These results suggest that the AAC-11 antiapoptotic pathway is upregulated in cells that offer an optimal environment for HIV-1 replication.

We sought to antagonize the action of AAC-11 by using a panel of synthetic peptides derived from the LZ domain located in its alpha helix 18 (19) fused to a cell-penetrating sequence of the antennapedia protein of *Drosophila melanogaster* (also commonly known as penetratin and referred to as RK16 here) (Fig. 2a), which can be

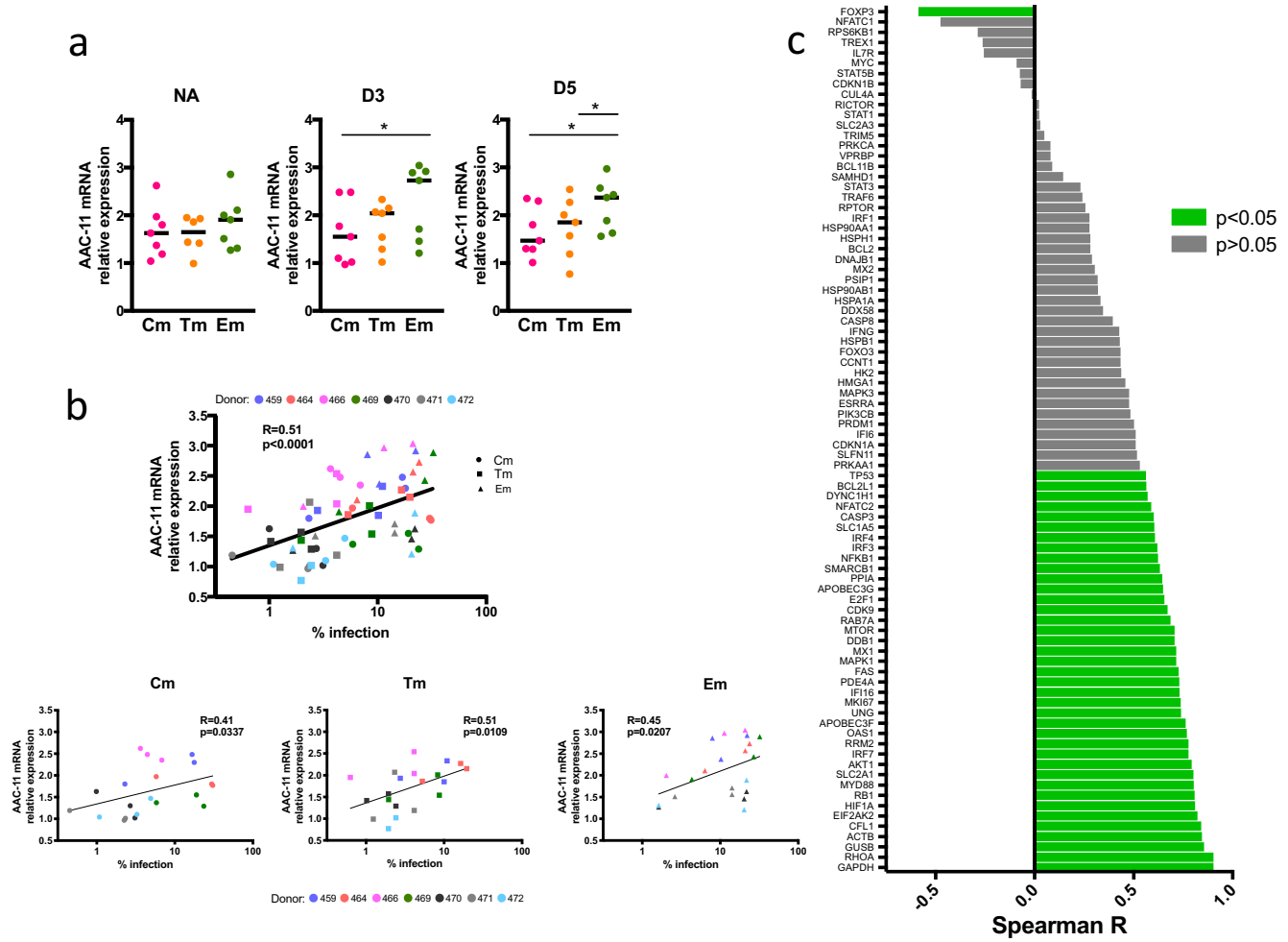

FIG 1 AAC-11 gene expression correlates with the proportion of infection in each memory CD4+ T cell subset and is associated with expression of various cell cycle and metabolism genes. (a) Nonactivated (NA) or activated (day 3 [D3] and 5 [D5]) CD4+ T cell memory subsets (Cm, Tm, and Em) were analyzed for the expression of AAC-11 at the time of infection. Medians are indicated by horizontal lines. (b) Nonactivated or activated (day 3 and 5) Cm, Tm, and Em subsets were analyzed for levels of AAC-11 gene expression and correlated with the percentage of infected cells in each subset at day 3 postinfection. (c) Correlation of AAC-11 gene expression with other genes in a 96-gene array. Bars indicate positive and negative Spearman correlation coefficients. *, $P \leq 0.05$.

used as an intracellular delivery method for its cargo (43). These AAC-11-derived peptides act as competitive inhibitors of protein-protein interactions, can prevent AAC-11 antiapoptotic activities, and have shown antitumor activities *in vitro* and *in vivo* (23–25). RT53 spanned the entire length of the AAC-11 LZ domain (Fig. 2a), and the other peptides spanned progressively smaller regions of the LZ domain. We applied these peptides to activated primary human CD4+ T cells (44) immediately after infection with HIV-1 and measured infection levels 3 days later (Fig. 2b). AAC-11-derived peptides reduced HIV-1 infection in a concentration-dependent manner (Fig. 2c). Shorter peptides were less effective at inhibiting infection (Fig. 2c and d). RK16, the penetratin, alone did not show any antiviral effect even at the highest concentration tested. We observed a rapid drop in the proportion of infected cells at a 6 μM peptide concentration for RT53 and RT39, the peptides exhibiting the strongest antiviral effects. At this concentration, RT53 was most potent at suppressing infection (50% effective concentration [EC_{50}] = 4.19 μM) (Fig. 2d), indicating that the entire length of the LZ domain of AAC-11 was necessary for full peptide potency. We, therefore, proceeded to work with RT53 at a 6 μM concentration.

We next tested if RT53 was able to inhibit infection of distinct HIV-1 strains (Fig. 3a). Both strains R5 (Bal) and X4 (NL4.3), as well as primary isolates (BX08, DH12, and 132w)

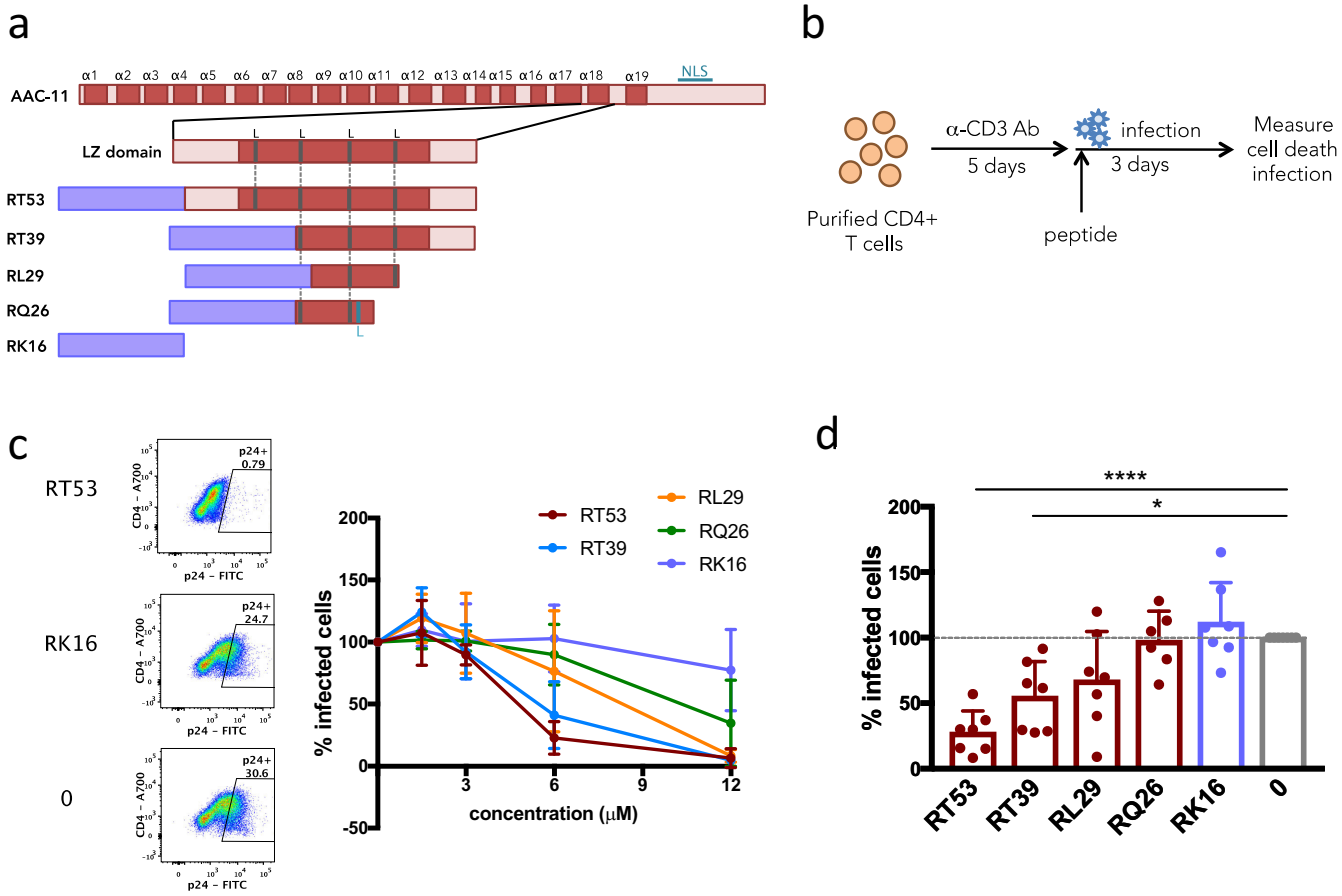

FIG 2 AAC-11-derived peptides inhibit HIV-1 infection. (a) Schematic representation of AAC-11-derived peptides showing the LZ domain. NLS, nuclear localization signal. (b) Experimental scheme of treatment of infected cells with AAC-11-derived peptides. (c) (Left) Representative flow cytometry plot of p24 staining in live untreated cells (0) or cells treated with 6 μM RT53 or RK16. (Right) Dose-response curve of the effect of AAC-11-derived peptides on HIV-1 infection in living cells. (d) Proportion of infection compared to nontreated control among living cells infected with HIV-1 Bal and treated with 6 μM the indicated peptides. *, $P \leq 0.05$; ****, $P \leq 0.0001$.

and single-cycle vesicular stomatitis virus glycoprotein (VSVG)-pseudotyped HIV-1 particles, were inhibited, albeit less efficiently for the last. RT53 was also able to inhibit *in vitro* infection of human CD4$^+$ T cells with SIV$_{mac251}$. Moreover, it inhibited viral spread from splenic CD4$^+$ T cells of cynomolgus macaques previously infected with SIV$_{mac251}$ (Fig. 3a). The inhibition of infection in both human and macaque cells is coherent with the high conservation of AAC-11 across species (20) and 100% homology between humans and macaques. Again, RK16 alone had no inhibitory effect on any of the viruses tested. Overall, our results showed that AAC-11-derived peptides were able to impair HIV-1 and SIV infection of CD4$^+$ T cells *in vitro*, as well as spread from *in vivo*-infected CD4$^+$ T cells.

Blockage of HIV-1 infection by AAC-11-derived peptides is associated with cell death. Since the AAC-11 peptides have been shown to induce cytotoxicity in cancer cells (21), we next evaluated the amount of cell death in our cultures. Indeed, we saw that all the peptides caused various rates of cell death (Fig. 4a). Moreover, we found that the proportions of cell death caused by different peptides in different donors were negatively correlated with the proportions of HIV-infected cells in the cultures (Fig. 4b). As before, RT53 was most potent at causing cell death. Interestingly, RT53 induced similar death rates in cells infected with various HIV-1 strains and in cells that had not been challenged with HIV-1 (Fig. 3b and 4a). This indicated that some CD4$^+$ T cells had preexisting sensitivity to the action of the peptides that was not dependent on infection.

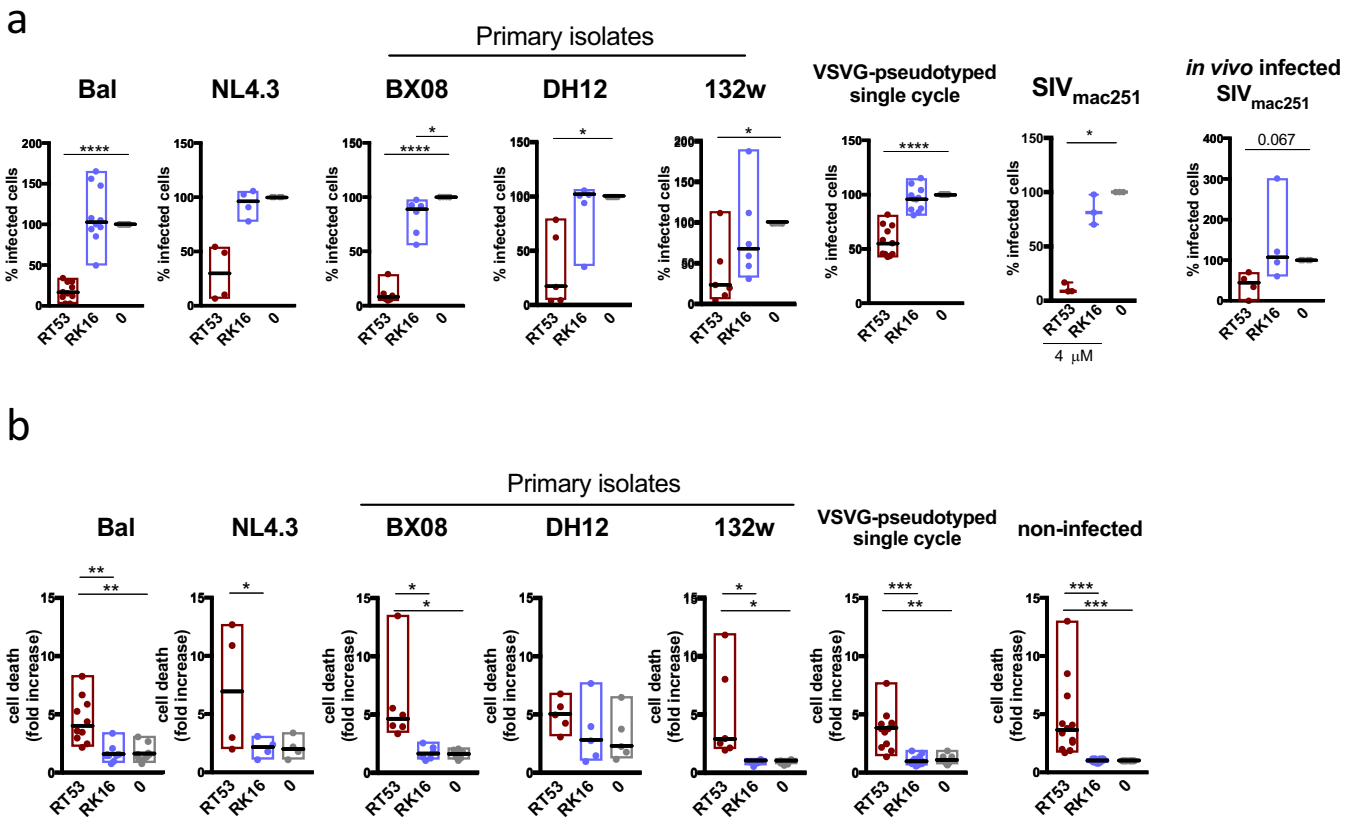

FIG 3 RT53 inhibits infection of diverse HIV-1 strains and SIV. Activated primary CD4+ T cells were infected with different HIV-1 strains and incubated with 6 μM RT53 or RK16 for 3 days. (a) Infection was measured by flow cytometry (intracellular p24) or ELISA (p24/p27) in supernatants. (b) Cell death was measured by flow cytometry (LIVE/DEAD violet viability dye). Values are expressed as a range (minimum-maximum) with medians indicated. Each symbol represents experiments with cells from a different donor. *, $P \leq 0.05$; **, $P \leq 0.01$; ***, $P \leq 0.001$; ****, $P \leq 0.0001$.

To explore the specificity of action of AAC-11-derived peptides, we analyzed if RT53 induced cell death in other cell types. We found that CD8+ T cells were susceptible to the action of RT53, although to a lesser extent than CD4+ T cells ($P = 0.039$), while NK cells were resistant to the cytotoxicity of RT53 ($P = 0.0078$) (Fig. 4c). Therefore, RT53 did not have a general cytotoxic effect on all lymphocytes. On the other hand, RT53 induced cytotoxicity in highly susceptible Jurkat and SupT1 human CD4+ T cell lines, but it did not affect the proportion of infected cells (data not shown), not recapitulating the selective effect observed in primary CD4+ T cells, further suggesting that the link between peptide-induced cytotoxicity and antiviral activity is due to particular properties of primary CD4+ T cells that favor HIV replication.

Together, these results show that AAC-11 did not exert a nonspecific cytotoxic action but affected particular cell subsets. Primary CD4+ T cells preferentially targeted by HIV-1 for infection had enhanced sensitivity to the actions of AAC-11-derived peptides. Hence, AAC-11-derived peptides may induce selective elimination of HIV-1 target cells.

Cell death induced by AAC-11-derived peptides is associated with K+ efflux and mitochondrial depolarization. We next investigated the mechanism of the RT53-mediated effect. We started by evaluating the kinetics of RT53 action. We used real-time flow cytometry to read out changes in several molecular indicators associated with cell death as a function of time (45). We found that treatment of cells with RT53 induced a sharp and rapid increase in the surface levels of phosphatidylserine (PS) (as determined by binding to annexin V-fluorescein isothiocyanate [FITC]), classically associated with apoptosis induction (Fig. 5a). Additionally, in a subset of RT53-treated CD4+ T cells, we also observed decreases in the intracellular levels of K+ ions (revealed

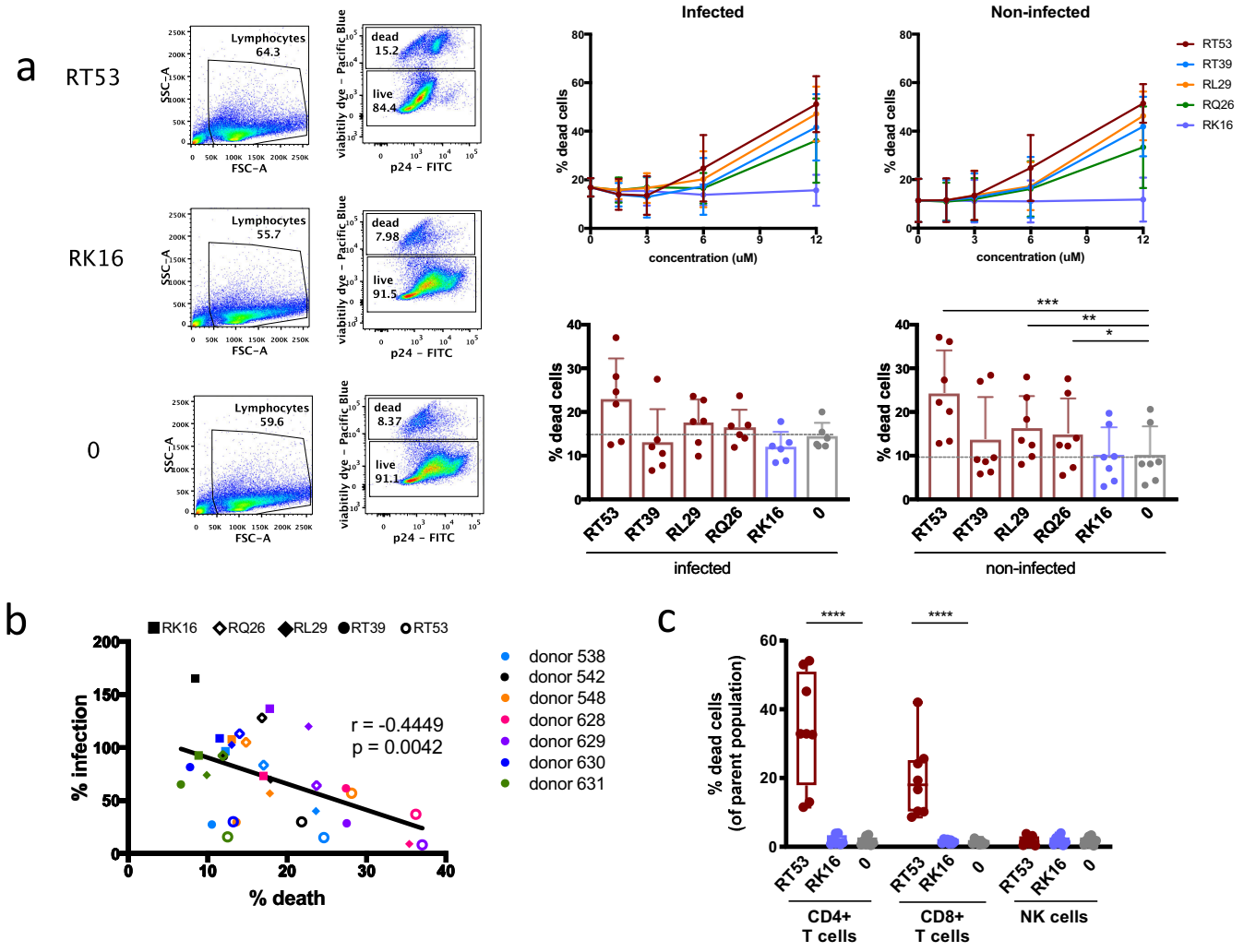

FIG 4 Decrease in HIV-1 infection is associated with cell death. (a) Example of flow cytometry gating strategy to evaluate cell death in cultures. *In vitro*-activated primary CD4$^+$ T cells were incubated with various concentrations of AAC-11-derived peptides after infection with HIV-1 Bal, and cell death was evaluated by flow cytometry on day 3 of infection. (b) Proportions of infected cells among live cells versus cell death in different donors' CD4$^+$ T cells incubated with 6 μM the indicated peptides. (c) PBMCs were treated with 6 μM RT53 or RK16 for 5 h, washed, stained for markers of CD4$^+$ CD8$^+$ T cells and NK cells and viability dye, and assessed by flow cytometry. The bars represent the minimum-maximum range, with medians indicated. Each symbol represents experiments with cells from a different donor. *, $P \leq 0.05$; **, $P \leq 0.01$; ***, $P \leq 0.001$; ****, $P \leq 0.0001$.

by the fluorescent K$^+$ indicator asanate potassium green 2 [APG-2]), the efflux of which has been linked to the activation of the cell death machinery (46–48), and in mitochondrial depolarization, evaluated by the increase in green fluorescence of the mitochondrial membrane potential dye JC-1 (Fig. 5a). These events were accompanied by an increase in DNA labeling with 7-aminoactinomycin D (7-AAD), a classical marker for dead cells. Cell death peaked at 30 min after treatment with the RT53 peptide in both noninfected and infected cells, with no significant increase at later time points (Fig. 5b).

To investigate if cell death caused by the peptides was indeed responsible for the observed antiviral effect, we sought to revert RT53-induced cytotoxicity by antagonizing intracellular K$^+$ efflux with increasing KCl concentrations in the culture medium (49). Noninfected CD4$^+$ T cells or cells that had been preinfected with VSVG-pseudotyped HIV particles were incubated with RT53 or RK16 for 5 h in the presence of increasing extracellular K$^+$ concentrations of up to 100 mM KCl supplementing the cell culture medium (Fig. 5c). We observed a KCl concentration-dependent decrease in RT53-mediated cell death relative to the RK16-treated or untreated condition, which

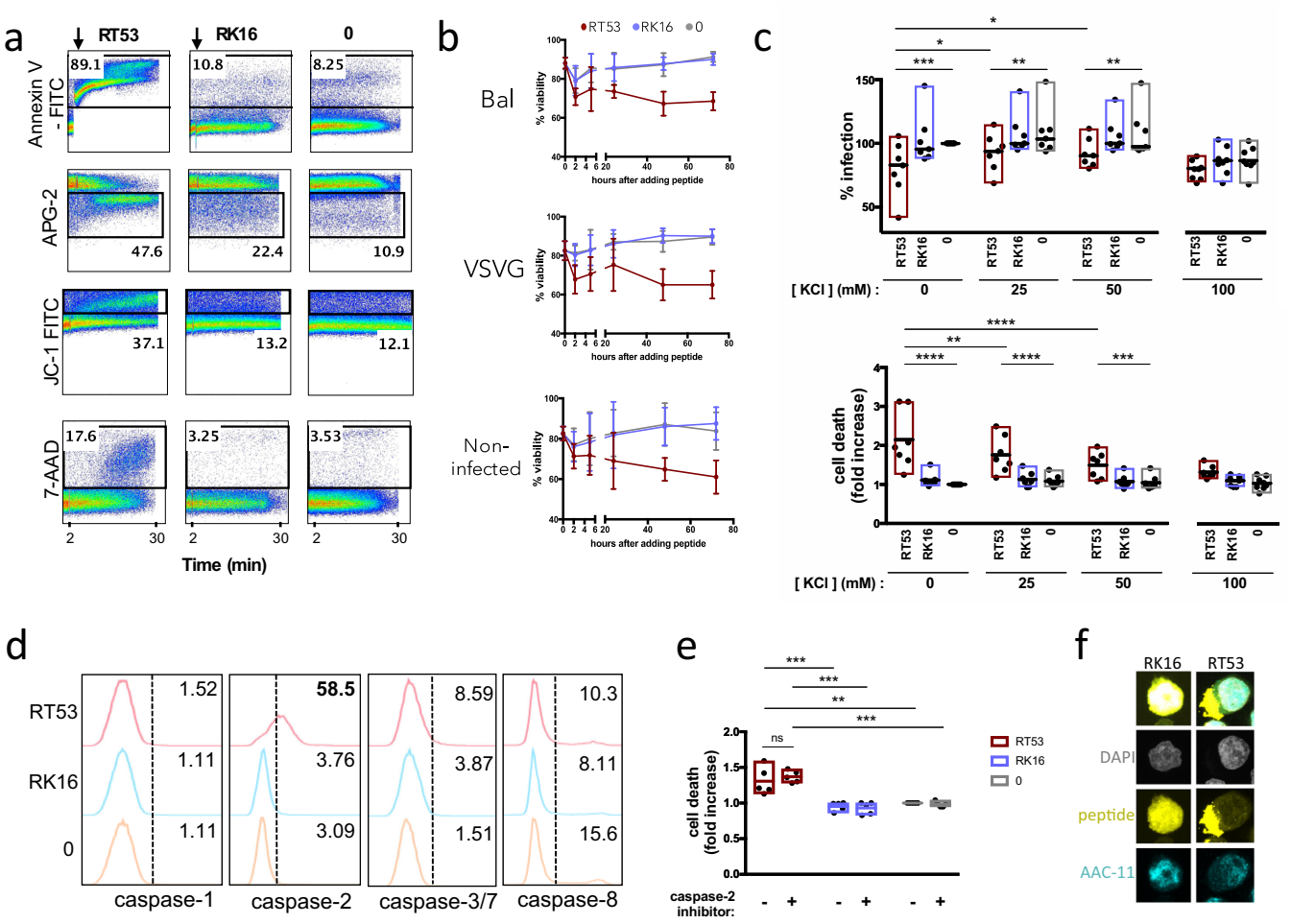

FIG 5 RT53-mediated cell death is rapid and is associated with K^+ efflux and mitochondrial depolarization. (a) Cells were placed in annexin V-FITC and 7-AAD staining buffer or loaded with a fluorescent K^+ indicator (APG-2) or a mitochondrial membrane potential probe (JC-1) and run on a flow cytometer to acquire fluorescence over time. The time point of peptide addition (after 2 min of acquisition) is indicated with an arrow. (b) Infected cells were incubated with 6 μM RT53 or RK16, and viability was determined with trypan blue at the indicated time points. (c) Cells preinfected with VSVG-pseudotyped HIV-1 particles (day 3 of infection) were incubated with 6 μM RT53 or RK16 in the presence of various concentrations of KCl for 5 h. Infection and cell death were then evaluated by flow cytometry. The symbols represent experiments with cells from different donors. The bars represent the minimum-maximum range, with medians indicated. (d) Cells were incubated with 6 μM RT53 or RK16 for 2 h and stained with probes for active caspases. (e) Cells were incubated with caspase 2 FAM-VDVAD-FMK probe and pulsed with 6 μM RT53 or RK16. Cell death was measured 5 h later by flow cytometry. (f) Immunofluorescent detection of RT53/RK16-Rd and AAC-11 in CD4+ T cells. Cells were incubated with 6 μM RT53/RK16-Rd for 2 h, washed, immobilized on polylysine-coated coverslips, fixed, and stained with antibodies for AAC-11 and DAPI. *, $P \leq 0.05$; **, $P \leq 0.01$; ***, $P \leq 0.001$; ****, $P \leq 0.0001$.

was accompanied by a progressive increase in the proportion of infected CD4+ T cells recovered at the end of culture. No differences were observed in the rates of cell death and the percentages of infected cells between RT53 and RK16 or a control when the cultures were done in the presence of 100 mM KCl, although we note that at this concentration, the rates of infection were overall lower than in CD4+ T cells cultured in the absence of extra KCl (Fig. 5c).

We then evaluated if RT53 treatment had an impact on the activation of caspases, known activators and effectors of cell death. Of note, caspase 2 has been recently reported to be repressed by AAC-11 (22). Upon treatment with the AAC-11-derived peptide, we did not observe significant activation of caspase 1, caspase 3/7, and caspase 8, but we saw strong activation of caspase 2 (Fig. 5d). Nevertheless, inhibition of caspase 2 activation did not lead to a decrease in cell death (Fig. 5e), suggesting that activation of caspase 2 was not the main mechanism responsible for cell death in our system. Similar results were obtained with inhibition of caspase 1, caspase 3/7, and caspase 8 (data not shown). These results are in agreement with a caspase-independent mechanism of cytotoxicity induced by RT53 in cancer cells (24).

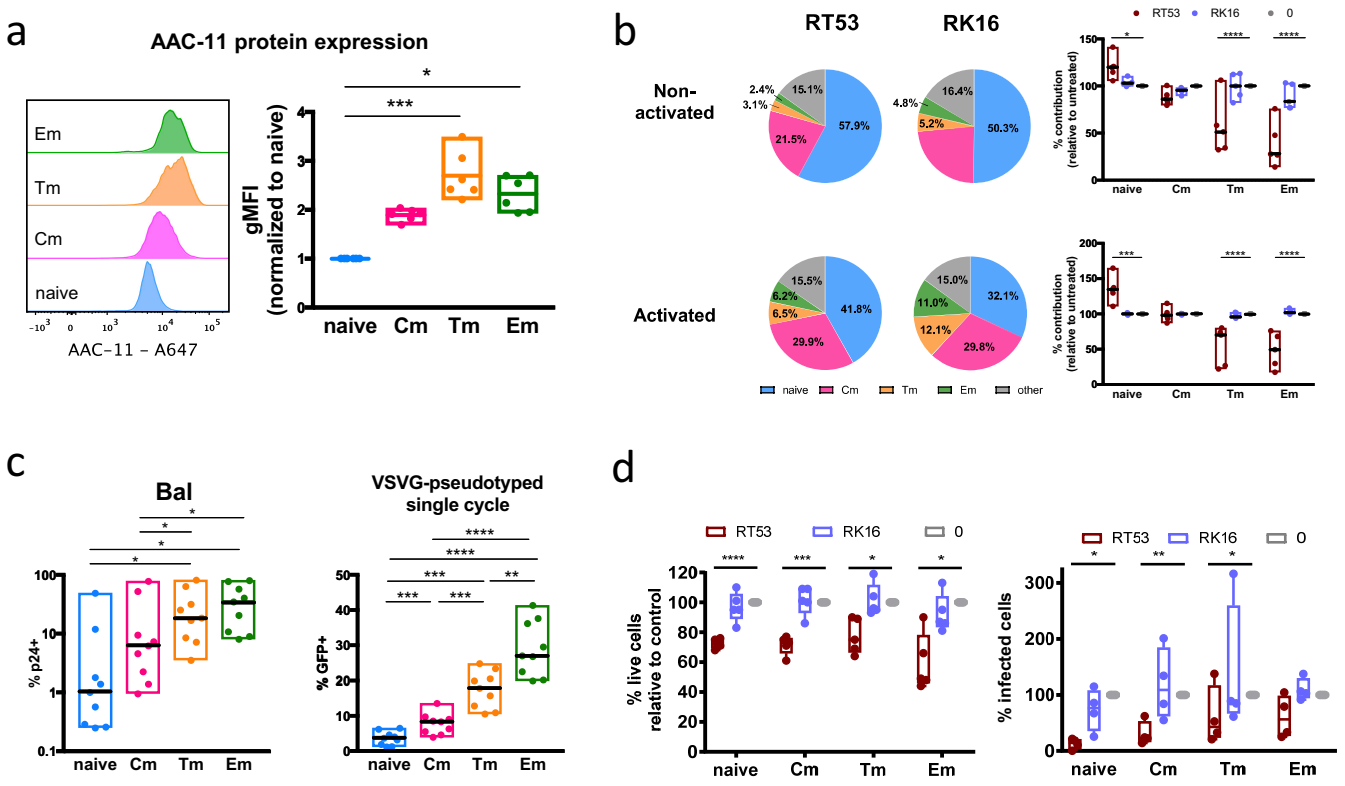

FIG 6 RT53 preferentially targets Tm and Em cells to cell death. (a) *In vitro*-activated CD4$^+$ T cells were stained for markers of CD4$^+$ T cell memory subsets and AAC-11. (b) *In vitro*-activated or nonactivated CD4$^+$ T cells were pulsed with 6 μM RT53 or RK16 for 5 h, harvested, and stained for markers of CD4$^+$ T cell memory subsets. (c) Levels of HIV-1 Bal or VSVG-pseudotyped single-cycle HIV particle infection were quantified by intracellular p24 staining in different CD4$^+$ T cell subsets by flow cytometry. (d) *In vitro*-activated CD4$^+$ T cells were sorted by FACS into naive, Cm, Tm, and Em subsets. Each subset was pulsed with 6 μM RT53 or RK16 for 24 h, and viability was measured by flow cytometry with LIVE/DEAD violet viability dye. In parallel, sorted cells were infected with HIV-1 Bal in the presence or absence of HIV-1 Bal, and rates of infection were determined on day 3 postinfection by intracellular p24. Viability and infection levels are expressed in relation to the untreated condition for each individual. *, $P \leq 0.05$; **, $P \leq 0.01$; ***, $P \leq 0.001$; ****, $P \leq 0.0001$.

RT53 was previously shown to mediate its cytotoxic effect through a membranolytic action by means of interaction with an unknown AAC-11 partner (23, 24). We therefore determined the cellular localization of RT53 and RK16 conjugated to rhodamine (Rd). As expected, RK16-Rd was found in the cytoplasm of the CD4$^+$ T cells (Fig. 5f), while RT53-Rd localized predominantly to the cell membrane. These studies were carried out at a 6 μM peptide concentration, but similar results were found at subcytotoxic peptide concentrations of 2 and 4 μM (data not shown). Therefore, our results indicate that, similar to cancer cells, RT53 could be causing cell death in primary CD4$^+$ T cells by membranolytic action.

Overall, our results show that RT53 induced rapid cell death in a subset of CD4$^+$ T cells, possibly through a membranolytic mechanism. The impairment of peptide-induced cell death abrogated the antiviral activity of the peptides, which provides a direct link between the peptide cytotoxic effect and its capacity to inhibit HIV infection.

RT53 preferentially depletes effector and transitional memory CD4$^+$ T cell subpopulations. Our previous results showed that AAC-11 mRNA expression was upregulated with CD4$^+$ T cell differentiation (Fig. 1). We have now found that the expression of AAC-11 at the protein level also increased with T cell differentiation (Fig. 6a). We therefore wondered if RT53 might have distinct impacts on different CD4$^+$ T cell subsets. RT53 treatment changed the relative contribution of CD4$^+$ T cell subsets to the total pool of CD4$^+$ T cells compared to nontreated or RK16-treated conditions (Fig. 6b). Naive CD4$^+$ T cells were enriched upon treatment with RT53, while the more differentiated Tm and Em CD4$^+$ T cells were depleted. Although activation *in vitro* changed the relative contribution of CD4$^+$ T cell subsets to the pool of CD4$^+$ T cells

somewhat, RT53 had similar impacts on CD4$^+$ T cell subsets when we used nonactivated or *in vitro*-activated cells (Fig. 6b). As previously reported (7), under our experimental conditions, naive CD4$^+$ T cells were highly resistant to infection with both VSVG-pseudotyped HIV-1 particles and HIV-1 Bal (Fig. 6c). Susceptibility to infection increased with T cell differentiation, with Em and Tm cells showing the highest infection levels (Fig. 6c). Thus, our results showed that RT53 preferentially targeted differentiated memory cells, which had heightened susceptibility to HIV infection.

However, not all Em and Tm cells were depleted after RT53 treatment, and some extent of peptide-induced cell death could also be observed in other CD4$^+$ T cell subsets, including naive cells. We therefore separately tested the impacts of RT53 treatment on isolated naive, Cm, Tm, and Em CD4$^+$ T cells. We confirmed that RT53 induced cell death in each of the CD4$^+$ T cell subsets (Fig. 6d). Moreover, RT53 treatment decreased HIV-1 infection in all CD4$^+$ T cell subsets. Overall, these results show that RT53 targeted cells with specific characteristics that were strongly enriched, but not exclusively found, within more differentiated subsets. Of note, the cells targeted by RT53 within each subset were susceptible to HIV-1 infection.

RT53 targets metabolically active cells. We next aimed to identify the characteristics of the CD4$^+$ T cells that were sensitive to the cytotoxic action of RT53. RT53 was previously shown to induce death of cancer cells during metabolic stress (50). Cancer cells rely on a high level of metabolic activity for adequate supply of biosynthetic intermediates for their life cycle, and similar conditions favor HIV-1 replication in CD4$^+$ T cells (7). We therefore analyzed if the differential sensitivities of CD4$^+$ T cells to RT53 treatment were related to differences in cellular metabolism. Following treatment of CD4$^+$ T cells with RT53, but not RK16, we observed the disappearance of larger CD4$^+$ T cells (determined by forward scatter [FSC] in flow cytometry) (Fig. 7a) and a decrease in the proportions of CD25^{high} and HLA-DR^{high} cells (Fig. 7b). We next analyzed the metabolic activity (glycolysis, measured by the extracellular acidification rate [ECAR], and oxidative phosphorylation [OXPHOS], measured by the oxygen consumption rate [OCR]) of living CD4$^+$ T cells in nontreated cells or cells treated with RT53/RK16 peptide (Fig. 7c). We found that the cells that survived RT53 treatment had lower mitochondrial respiration (spare respiratory capacity) and glycolysis {basal ECAR and glycolytic reserve [ΔECAR after addition of the uncoupler of mitochondrial oxidative carbonyl cyanide 4-(trifluoromethoxy)phenylhydrazone (FCCP)]} than cells that had not been treated or were treated with RK16 (Fig. 7d). We therefore concluded that CD4$^+$ T cells with the highest metabolic activity were more sensitive to the action of AAC-11-derived peptides.

RT53 depletes the pool of cells permissive to HIV-1 replication. To further confirm that RT53 was killing HIV-1-susceptible target cells and selecting for cells resistant to viral replication, we treated activated CD4$^+$ T cells with RT53 or RK16 for 24 h, sorted live cells from dead cells, and infected the sorted live cells (Fig. 8a). We found that the cells that survived RT53 treatment were less susceptible to both HIV-1 Bal and VSVG-pseudotyped HIV-1 particles (Fig. 8a), although the inhibition was more marked for the fully competent virus. Importantly, we did not see any further increase in cell death compared to control conditions in sorted living cells.

We next sought to determine which stage of the viral replication cycle was blocked in cells surviving RT53 treatment. RT53 induced a decrease in the proportion of CCR5^{high} cells (Fig. 8b), although this difference did not appear sufficient to explain the level of HIV inhibition found. Moreover, RT53 did not change CCR5 cell surface distribution in the cells that survived treatment with RT53 (Fig. 8b). RT53 was still able to block infection when added 24 h after the culture of CD4$^+$ T cells with HIV-1 Bal (Fig. 8d). We next measured the levels of total (as a measure of reverse transcription) and integrated viral DNA at various time points postinfection with VSVG-pseudotyped HIV-1 particles in RT53/RK16-treated or untreated cells (Fig. 8e). The levels of both total and integrated HIV-1 DNA drastically increased as a function of time in RK16-treated and untreated cells, but not in RT53-treated cells. These results indicate that the virus is unable to complete early steps of its life cycle in cells surviving RT53 treatment and that these cells are nonpermissive to viral

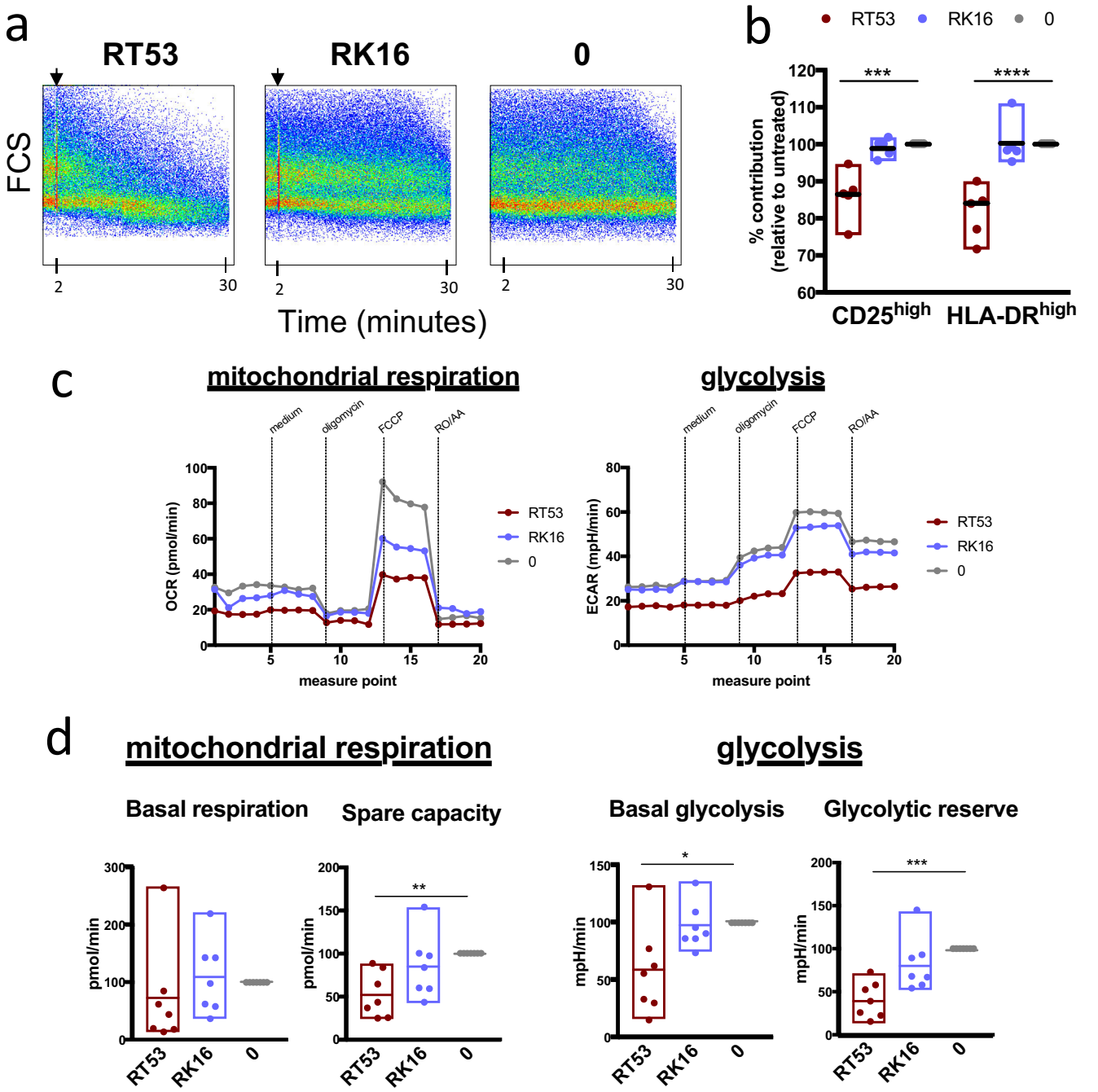

FIG 7 RT53 preferentially targets activated and most metabolically active cells. (a) Example of RT53 treatment preferentially targeting large cells (evaluated by the FCS parameter by real-time flow cytometry). (b) *In vitro*-activated cells were pulsed with 6 μM RT53 or RK16 for 5 h. The relative surface expression of CD25 and HLA-DR by flow cytometry compared to the no-peptide condition is shown. (c) OCR and ECAR values of CD4$^+$ T cells from one representative donor. (d) Relative basal mitochondrial respiration (basal respiration), spare mitochondrial capacity (spare capacity), basal glycolysis (basal ECAR), and glycolytic reserve (ECAR after FCCP) obtained with cells from 7 donors compare to the no-peptide condition (0). Values are expressed as a minimum-maximum range, with medians indicated. *, $P \leq 0.05$; **, $P \leq 0.01$; ***, $P \leq 0.001$; ****, $P \leq 0.0001$.

replication. Thus, RT53 treatment killed cells in which the virus was able to establish productive infection while allowing the survival of HIV-1-resistant cells.

DISCUSSION

In this study, we showed that peptides derived from the LZ region of the antiapoptotic factor AAC-11 inhibited HIV-1 infection of primary CD4$^+$ T cells. In particular, we

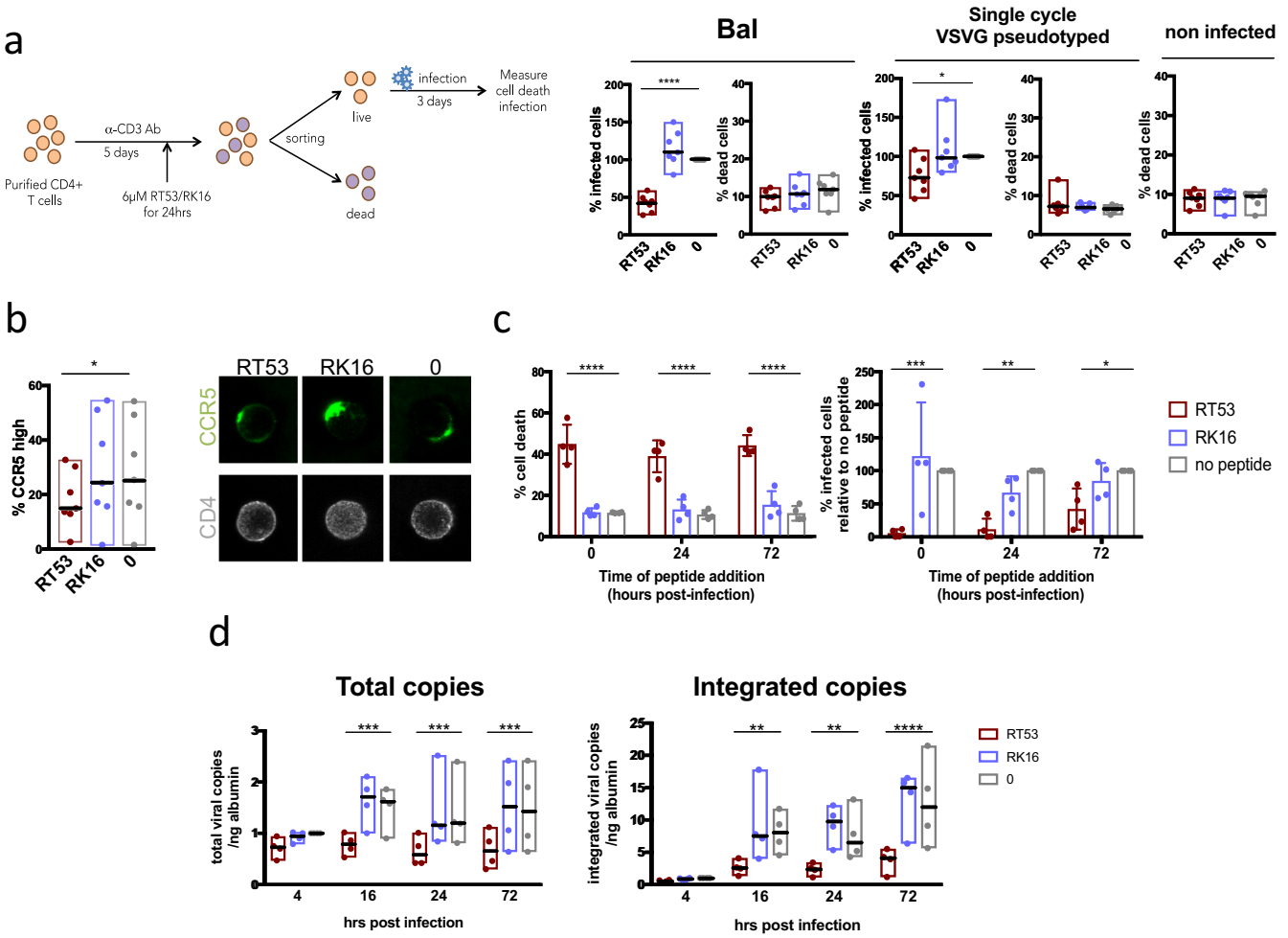

FIG 8 RT53-surviving cells are resistant to HIV infection. (a) *In vitro*-activated CD4+ T cells were incubated with 6 μM RT53 or RK16 for 24 h. Live cells were then sorted from dead cells using FACS, and the live cells were infected with the indicated HIV-1 strains. Cell death and infection were evaluated by flow cytometry 3 days later. (b) Proportion of CCR5^{high}-expressing cells and CCR5 cell surface distribution among *in vitro*-activated CD4+ T cells after 5 h of treatment with 6 μM RT53 or RK16. (c) Antiviral effect of RT53 when added at different times after infection. Activated CD4+ T cells were infected with HIV-1 Bal, and 6 μM RT53 or RK16 was added at the indicated times postinfection. The levels of cell death and infection were quantified by flow cytometry on day 3 postinfection. (d) Total and integrated viral copies evaluated at various time points postinfection in cells infected with VSVG-pseudotyped HIV-1 particles and treated with 6 μM RT53 or RK16. The values are normalized to the untreated condition 4 h postinfection and expressed as minimum-maximum ranges with medians indicated. *, $P \leq 0.05$; **, $P \leq 0.01$; ***, $P \leq 0.001$; ****, $P \leq 0.0001$.

found that RT53 was able to block infection with a large panel of laboratory-adapted and primary viral strains by inducing the death of CD4+ T cells that offered the best conditions to sustain HIV-1 replication.

Although sensitivity to RT53 was more pronounced in highly differentiated CD4+ T cell subsets, RT53 treatment eliminated a fraction of the cells within each cell subset, rendering the remaining cells resistant to HIV-1 replication. RT53 depleted highly metabolic cells, which is in agreement with the observation that a rich metabolic environment is necessary for HIV replication (7). Upon antigenic stimulation, CD4+ T cells upregulate their metabolic activities, in particular glucose metabolism, to cope with the bioenergetic demands necessary to perform their functions. Thus, naive and central memory CD4+ T cells are typically smaller and have decreased metabolic activities compared to more differentiated and activated subsets. However, we have recently shown that some cells with enhanced metabolic activity can be found even among phenotypically quiescent naive T cells and that these cells are susceptible to HIV-1 infection (7). Here, we found that there was a close association between AAC-11 peptide-induced cell death and inhibition of HIV infection. Not only did the rates of cell

death induced by AAC-11 peptides correlate with the extent of HIV inhibition, but precluding cell death by increasing extracellular levels of K^+ also restored the infectibility of $CD4^+$ T cells. Cellular metabolism and cell death are deeply entangled. Metabolic arrangements are necessary to sustain long-term memory cells. External signals provided by T cell receptor activation or growth factors, such as interleukin 2 (IL-2) and IL-7, promote an antiapoptotic state of the cell by increasing the levels of metabolite transporters (e.g., Glut1) that ensure the supply of nutrients necessary to sustain the bioenergetic demands of the cell (51, 52). The absence of these signals provokes a limitation in the influx of nutrients that results in metabolic stress and the activation of cell death pathways. Our results indicate that AAC-11-derived peptides may tilt the equilibrium of highly metabolic cells toward cell death, even among less differentiated cells with a stronger antiapoptotic basal state.

Although the antiapoptotic action of AAC-11 is well documented, the molecular mechanisms underlying its activity are still unclear. AAC-11 possesses several domains predicted to be responsible for protein-protein interactions (19), and its expression may interfere with different mechanisms of cell death. The peptides that we tested here were designed to mimic the heptad leucine repeat region of AAC-11 and to be used as competitive inhibitors that abrogate the interaction of AAC-11 with its partners. In tumor cells, physical interaction between the LZ domain of AAC-11 and Acinus prevents Acinus proapoptotic cleavage by caspase 3. In our study, we did not observe significant changes in the expression of Acinus upon treatment with AAC-11-derived peptides (data not shown), and caspase 3 activity was not significantly detected under our experimental conditions, suggesting that this pathway was not the major contributor to the T cell death observed in our experiments. In contrast, we found that treatment with RT53 induced a strong increase in caspase 2 activity. Although AAC-11 has been shown to physically bind to the caspase recruitment domain of caspase 2, preventing its autocleavage (22), the activation of this caspase seen in our experiments was probably due to a side effect of the decrease in intracellular K^+ levels caused by the peptides (22, 53). The inhibition of caspase 2 activity also did not lead to the restoration of cell viability, suggesting that the mechanism of cell death induced by RT53 is independent of caspase 2 activation. RT53 was previously seen to localize to the plasma membrane compartment of cancer cells and was reported to have a membranolytic mechanism of action. We have also observed the peptide's localization to this cellular compartment in primary $CD4^+$ T cells. The fast kinetics of the peptide's activity also point to action through rearrangement of preexisting cellular factors probably found at the cell's plasma membrane and enriched in metabolically active cells.

Previous analyses have ruled out the nonspecific detergent-like cell death mechanism of RT53 (24). Indeed, we also found here that RT53 was cytotoxic to only some subsets of peripheral blood mononuclear cells (PBMCs), thus confirming the specificity of RT53 action, possibly through a membrane partner absent from certain cells. Interestingly, we also observed that RT53 did not have an antiviral effect despite observable cytotoxicity in the $CD4^+$ Jurkat and SupT1 T cell lines. Immortalized cell lines are known to have perturbed survival and metabolic pathways, thus providing a more favorable molecular environment for HIV-1 replication. This observation also points to the existence of a specific survival pathway used by HIV-1 in primary $CD4^+$ T cells perturbed by RT53.

Of note, although we observed consistent inhibition of infection with VSVG-pseudotyped HIV-1 single-cycle particles upon treatment with AAC-11 peptides, the inhibition was more important when we used wild-type (WT) viruses, either R5 or X4. There are several possible explanations for this. First, the additional block to HIV infection observed when we used WT viruses could be due to a cumulative effect of multiple infection cycles. Second, cells selected upon treatment with AAC-11 may be more resistant to WT virus. For instance, some cells expressing high levels of CCR5 were depleted upon treatment with RT53. We also cannot exclude the possibility that treatment with AAC-11-derived peptides induced further viral restriction in the cells that survived. Finally, infection with WT HIV might induce cellular changes that could

increase the susceptibility of infected cells to the action of AAC-11-derived peptides. For instance, HIV has been shown to induce metabolic changes in infected cells and, in particular, an increase in the expression of Glut1 to -3 (54).

Our results showed that AAC-11-derived peptides were active against CD4$^+$ T cells that were particularly susceptible to HIV-1 infection. It remains to be established if this sensitivity to the peptides remains in persistently infected cells. However, our results suggest that sensitivity to the action of RT53 decreased somewhat 72 h after infection, suggesting HIV-1-mediated modification of the cell death pathways in infected cells, as has been shown for macrophages (55). The mechanisms by which an infected cell persists are not completely clear, as HIV has cytopathic effects that lead to the death of infected CD4$^+$ T cells. It has been recently reported that persistent latently infected CD4$^+$ T cells in which the virus has been reactivated are intrinsically resistant to killing by HIV-specific CD8$^+$ T cells (56), which indicates that the persistent reservoir might be seeded in cells programmed to resist cell death. BIRC5 (also known as Api4 or survivin), a member of the inhibitor of apoptosis protein family, is upregulated in CD4$^+$ T cells during HIV-1 infection and contributes to the persistence of infected cells (57). Upregulation of BIRC5 on infected CD4$^+$ T cells was triggered by OX40, a costimulatory receptor that promotes T cell differentiation and survival (58, 59) and contributes to the metabolic boost necessary for T cell activation (60). It is thus possible that HIV-1 exploits/activates several cellular survival programs associated with T cell activation and metabolic activity to ensure its persistence.

Although further studies will be necessary to directly evaluate this, our results suggest that HIV-1 may rely on the AAC-11-dependent antiapoptotic pathway for the establishment of productive infection in CD4$^+$ T cells. AAC-11 gene expression, besides strongly correlating with multiple genes involved in the regulation of cell metabolism, was also correlated with the expression of RRM2 (Fig. 1c), an enzyme that is critical for the *de novo* synthesis of deoxynucleoside triphosphates (dNTPs) and the depletion of which blocks HIV-1 infection in macrophages and dendritic cells (42, 61). AAC-11 mRNA levels also correlated with the expression of other genes that have been associated with the HIV replication cycle, in particular, trafficking (i.e., CFL1, DYNC1H1, and ACTB) and transcription (i.e., CDK9 and NFKB1). This suggests that AAC-11-expressing cells may offer an ideal environment for HIV-1 replication. AAC-11 prevents apoptosis of tumor cells under conditions of nutrient deprivation and in the absence of growth factors. We can therefore speculate that the AAC-11 survival pathway might play a similar role in promoting persistence of memory CD4$^+$ T cells and HIV infection. Like the mechanisms associated with HIV persistence, it is also unclear how some T cells survive to become long-lived memory cells. While most T cells undergo apoptosis at the end of the immune response when environmental signals wane, a few cells survive even in the absence of growth factors (62). We found that expression of the apoptosis-inhibitory protein AAC-11 increased with differentiation of memory CD4$^+$ T cells. Our results suggest that the AAC-11 survival pathway may be involved in the regulation of T cell immunity, a function that has not been previously described and deserves further detailed exploration.

Among current strategies under evaluation in pursuing a HIV cure, allogeneic hematopoietic stem cell transplantation has been shown to drastically reduce the viral reservoir (63). However, this is a risky intervention associated with severe immune ablation. We found that AAC-11 peptides blocked HIV infection through the preferential killing of "HIV-1-infectable" cells but preserved a significant fraction of T cell immunity, in particular, the less differentiated T cells. RT53 has been shown to be efficient *in vivo* in murine models of cancer with few adverse effects. Although its clinical application in the context of HIV infection remains uncertain, our results serve as a proof of concept that selective elimination of HIV-1 targets is a possible therapeutic strategy.

MATERIALS AND METHODS

Peptides, antibodies, and probes. Peptides (Proteogenix) were received as dry powder and reconstituted with water for use. The peptide sequences are as follows: RT53, RQIKIWFQNRRMKWKKAKLNAEKLKDFKIRLQYFARGLQVYIRQLRLALQGKT; RT39, RQIKIWFQNRRMKWKKLQYFARGLQVYIRQLRLALQGKT; RL29, RQIKIWFQNRRMKWKKYFARGLQVYIRQL; RQ26, RQIKIWFQNRRMKWKKLQYFARGLLQ; RK16, RQIKIWFQNRRMKWKK.

The antibodies and dyes used for flow cytometry and fluorescence-activated cell sorting (FACS) were as follows: LIVE/DEAD violet viability dye (ThermoFisher), CD3-phycoerythrin (PE) (clone SK7; Biolegend), CD4-A700 (clone OKT4; eBioscience), CD45RA-allophycocyanin (APC)-Cy7 (clone HI100; Biolegend), CCR7-PE-Cy7 (clone GO43H7; Biolegend), CD27-APC (clone M-T271; Miltenyi), CD25-PE-Dazzle 594 (clone M-A251; Biolegend), HLA-DR-peridinin chlorophyll protein (PerCP)-Cy5.5 (clone G46-6; Biolegend), CCR5-PE (clone 3A9; BD), and p24-FITC (clone KC57; Coulter). AAC-11 expression was analyzed by intracellular flow cytometry staining using a BD Cytofix/Cytoperm buffer set (BD) and anti-AAC-11 primary antibody (ab65836; Abcam) at 1/100 dilution, followed by a secondary antibody conjugated to A674 (ThermoFisher; A21244) at 1/1,000 dilution. Caspase activity was assayed with the following probes according to the manufacturer's instructions: caspase 1 660-YVAD-FMK probe (FLICA 660 caspase 1 assay kit; ImmunoChemistry Technologies LLC), caspase 2 6-carboxyfluorescein (FAM)-VDVAD-FMK probe (FAM-FLICA caspase 2 assay kit; ImmunoChemistry Technologies LLC), caspase 3/7 SR-DEVD-FMK probe (SR-FLICA caspase 3/7 assay kit; ImmunoChemistry Technologies LLC), and caspase 8 FAM-LETD-FMK probe (FAM-FLICA caspase 8 assay kit; ImmunoChemistry Technologies LLC). FACS was performed on a BD Aria and flow cytometry acquisition on a BD LSRII.

Isolation and culture of primary human CD4$^+$ T cells. Healthy donor blood prepared as a buffy coat was obtained from Etablissement Français du Sang (EFS) (agreement with Institut Pasteur C CPSL UNT, 15/EFS/023). The blood was overlaid on Ficoll (EuroBio) at a ratio of 2:1 (vol/vol) blood to Ficoll and centrifuged at 1,800 rpm for 30 min at minimum acceleration/deceleration to obtain PBMCs. CD4$^+$ T cells were then purified from the PBMCs by negative selection using a StemCell EasySep human CD4$^+$ T cell isolation kit. Cells were counted and cultured in RPMI 1640 containing Glutamax (ThermoFisher), 10% fetal bovine serum (FBS), penicillin-streptomycin (ThermoFisher; 100 U/ml), and IL-2 (Miltenyi; 100 U/ml) (referred to below as culture medium) at 10^6 cells/ml at 37°C in a 5% CO_2 humidified incubator. The cells were activated with soluble anti-CD3 (clone UCHT-1; Biolegend) for 5 days prior to infection or analysis as previously described (44).

Isolation and culture of primary infected macaque CD4$^+$ T cells. Macaque splenic CD4$^+$ T cells were obtained from cynomolgus macaques (*Macaca fascicularis*) that were imported from Mauritius and housed at Commissariat à l'Energie Atomique et aux Energies Alternatives (CEA), Fontenay-aux-Roses, France, in compliance with the Standards for Human Care and Use of Laboratory Animals (assurance number A5826-01). The animals were part of the pVISCONTI study, which received ethics approval under the number APAFIS#2453-2015102713323361 v2. They were infected intravenously with 1,000 animal infectious dose 50 (AID_{50}) of $SIVmac_{251}$ and sacrificed at a study endpoint, at which time spleen samples were obtained. The macaque splenic CD4$^+$ T cells were purified by mechanical disruption of a spleen sample in RPMI medium using a GengleMACS dissociator (Miltenyi) followed by cell overlay over Ficoll (EuroBio) (diluted with PBS to 90% prior to use) and centrifugation at 350 $\times$ *g* for 20 min. The cells were then subjected to red cell lysis and then to CD4$^+$ T cell negative selection using a CD4$^+$ T cell negative-selection kit (Miltenyi). The cells were cultured in culture medium overnight prior to incubation with peptides. Viral spread from *in vivo*-infected cells was monitored by enzyme-linked immunosorbent assay (ELISA) quantification of p27 (XpressBio) levels on culture supernatants.

Infection and peptide treatment of primary CD4$^+$ T cells. Activated CD4$^+$ T cells were infected with either Bal (2.9 ng/ml p24), BX08 (21 ng/ml p24), DH12 (3 ng/ml p24), 132w (6.3 ng/ml p24), NL4.3 (7 ng/ml p24), VSVG-pseudotyped Δ*env*-Δ*nef*-GFP (7 ng/ml p24) virus or SIV_{mac251} (36.7 ng/ml p27) by centrifuging at 1,200 $\times$ *g* for 1 h at room temperature and then incubating for 1 h at 37°C in a humidified 5% CO_2 incubator. The cells were then washed once with phosphate-buffered saline (PBS), incubated in culture medium, and treated with peptides at 6 μM concentration unless otherwise indicated. Cell death and infection were measured on day 3 postinfection unless otherwise stated. Cell death was evaluated using flow cytometry (LIVE/DEAD violet viability dye; ThermoFisher), and infection was evaluated by either flow cytometry (intracellular p24 staining) or p24/p27 ELISA (XpressBio).

Real-time flow cytometry. Cells were washed once with PBS and incubated in annexin buffer (10 mM HEPES, 140 mM NaCl, 2.5 mM $CaCl_2$, pH 7.4) in the presence of annexin V-FITC (Biolegend) at a concentration of 10^6 cells/ml for 15 min. 7-AAD (Biolegend) was added for the last 5 min of incubation. The cells were then directly passed through the flow cytometer to acquire fluorescence versus time without washing. Alternatively, cells were stained with APG-2 AM (Abcam), a fluorescent K^+ indicator, at a final concentration of 1 μM in plain RPMI 1640 medium for 30 min at room temperature, washed twice with plain RPMI 1640, resuspended in PBS at 10^6 cells/ml, and incubated with 7-AAD (Biolegend) for 5 min before acquisition. To measure mitochondrial membrane potential, cells were stained with JC-1 indicator (ThermoFisher) at a final concentration of 2 μM in PBS at 37°C for 15 min, washed once, and analyzed on a flow cytometer; 6 μM peptides was added after 2 min of baseline acquisition, and acquisition continued for an additional 28 min.

Caspase 2 inhibition. *In vitro*-activated CD4$^+$ T cells were pretreated with FAM-VDVAD-FMK caspase 2 inhibitor (ImmunoChemistry Technologies LLC) according to the manufacturer's instructions for 30 min at 37°C and then pulsed with 6 μM RT53 or RK16 for 5 h. Cell death and caspase 2 activity were evaluated by flow cytometry.

Immunofluorescence microscopy. Activated CD4$^+$ T cells were incubated with 6 μM RT53-rhodamine (rhodamine-RQIKIWFQNRRMKWKKAKLNAEKLKDFKIRLQYFARGLQVYIRQLRLALQGKT) or RK16-rhodamine (rhodamine-RQIKIWFQNRRMKWKK) (Proteogenix) for 2 h. The cells were then washed twice with PBS, immobilized on polylysine-coated coverslips, fixed with 4% paraformaldehyde for 10 min at room temperature, neutralized with 50 mM NH_4Cl for 10 min at room temperature, and washed twice with PBS. The cells were then permeabilized with 0.1% Triton X-100 in PBS for 5 min at room temperature. All antibody incubations were performed in 1% bovine serum albumin (BSA) in PBS. Intracellular

staining for AAC-11 was performed with anti-AAC-11 antibody (Abcam; ab65836) at 1/200 dilution for 1 h at room temperature, followed by anti-rabbit IgG-A647 secondary antibody (Life Technologies; A31573) at 1/400 dilution for 45 min at room temperature. The coverslips were then washed, stained with DAPI (4′,6-diamidino-2-phenylindole) for 15 min at room temperature, and mounted using Fluoromount G (ThermoFisher) mounting medium.

For analyses of CCR5 distribution, activated CD4$^+$ T cells were incubated with 6 μM RT53 or RK16 (Proteogenix) for 2 h. The cells were then washed twice with PBS, immobilized on polylysine-coated coverslips, fixed with 4% paraformaldehyde for 10 min at room temperature, neutralized with 50 mM NH_4Cl for 10 min at room temperature, and washed twice with PBS. All antibody incubations and washes were performed in 1% BSA in PBS. The cells were incubated with primary mouse anti-CD4 antibody (clone OKT4; Tonbo Biosciences; 70-0048-U100) and rabbit polyclonal anti-CCR5 (Abcam; ab7346) at 1/100 dilution for 1 h at room temperature, washed, and incubated with secondary antibodies (anti-mouse IgG-A488 [Life Technologies; A11029] and anti-rabbit IgG-A647 [Life Technologies; A31573]) at 1/1,000 dilution for 30 min at room temperature. The coverslips were then washed once in PBS and mounted using Fluoromount G (ThermoFisher) mounting medium.

Measurements of cellular metabolism. The OCR and ECAR were measured on a Seahorse XF96 analyzer using a Seahorse XF Cell Mito stress test kit (Agilent). Briefly, activated CD4$^+$ T cells were incubated with 6 μM RT53 or RK16 for 4 h at 37°C. The cells were then counted, washed in Seahorse XF medium (Agilent Seahorse XF base medium with 2 mM Glutamax [Agilent; 102365-100]) containing 10 mM glucose (Sigma), 2 mM sodium pyruvate (Life Technologies), and adjusted to pH 7.4. An equal number of live cells were seeded at 2×10^5 cells per well in XF96 V3 PS plates (Seahorse Bioscience) precoated with 0.5 mg/ml Corning Cell-Tack cell and tissue adhesive (Corning; 354240) and incubated for a minimum of 30 min in a CO_2-free 37°C incubator prior to acquisition. The following drugs were placed at injection ports: Seahorse XF medium (port A), 2.5 μM oligomycin (port B), 0.9 μM FCCP (port C), and 1 μM rotenone and 1 μM antimycin A (port D).

Quantitative RT-PCR. (i) Evaluating the expression of AAC-11 and other genes in CD4$^+$ T cell memory subsets. The expression levels of AAC-11 and other genes on CD4$^+$ T cell subsets were analyzed in a previous study (7, data set [doi:10.17632/vfj3r27gnf.1]). Briefly, the total RNA from 5×10^4 cells was extracted using an RNA trace kit (Macherey-Nagel), treated with DNase, reverse transcribed using reverse transcription master mix (Fluidigm), preamplified using PreAmp master mix (Fluidigm), and treated with exonuclease I (New England Biolabs). Samples were then mixed with SsoFast EvaGreen Supermix with Low ROX (Bio-Rad), DNA binding dye (Fluidigm), and assay mix (assay loading reagent [Fluidigm] and Delta Gene primers [Fluidigm]). The expression levels were read on a Biomark HQ system (Fluidigm). The expression levels of BECN1 were used for normalization. Gene expression values were plotted as $2^{-\Delta\Delta CT}$.

(ii) Evaluating the expression of viral gene products. Cells were collected by centrifugation, and the dry pellet was stored at −80°C until DNA extraction. DNA was extracted using a NucleoSpin tissue kit (Macherey-Nagel). Real-time PCR (RT-PCR) to quantify total and integrated HIV-1 DNA was performed as described previously (64) using TaqMan universal PCR master mix (ThermoFisher). Briefly, total viral DNA was quantified using the following primers and probe: CTTTCGCTTTCAAGTCCCTGTT (forward), AGATCCCTCAGACCCTTTTAGTCA (reverse), and FAM-TGGAAAATCTCTAGCAGTGGCGCCC-black hole quencher 1 (BHQ1) (probe). The 8E5 cell line containing a single viral copy per cell was used as a standard. Integrated viral DNA was quantified by first preamplifying the DNA using AccuTaq LA DNA polymerase (Sigma) and the following primers: AGCCTCCCGAGTAGCTGGGA (FirstAluF), TTACAGGCATG AGCCACCG (FirstAluR), and CAATATCATACGCCGAGAGTGCGCGCTTCAGCAAG (NY1R). A second DNA amplification round was performed with TaqMan universal PCR master mix (ThermoFisher) using the following primers: AATAAAGCTTGCCTTGAGTGCTC (NY2F), CAATATCATACGCCGAGAGTGC (NY2R), and FAM-AGTGTGTGCCCGTCTGTTGTGTGACTC-6-carboxytetramethylrhodamine (TAMRA) (NY2ALU probe). HeLa cells containing HIV-1 integrated DNA were used as a standard (64). The results were normalized to nanograms of actin using a human DNA standard (Sigma). The primers and probe used for quantification of actin were TGCATGAGAAAACGCCAGTAA (forward), ATGGTCGCCTGTTCACCAA (reverse), and FAM-TGACAGAGTCACCAAATGCTGCACAGAA-TAMRA (probe).

Statistical analysis. Statistical analysis was performed using GraphPad Prism software. Linked parametric or nonparametric one-way analysis of variance (ANOVA) or two-way ANOVA was used, depending on the experiment. Dunnett's, Dunn's, or Holm-Sidak's multiple-comparison tests were used for *post hoc* analysis.

ACKNOWLEDGMENTS

We thank all the blood donors for their generous contributions to research. Anastassia Mikhailova and Amal Elfidha were enrolled in the *école doctorale* Bio Sorbonne Paris Cité (BioSPC) for their Ph.D. programs. We acknowledge the Cytometry and Biomarker UTechS at Institut Pasteur and the personnel from the Infectious Disease Models and Innovative Therapies (IDMIT) platform for support in conducting the study.

Anastassia Mikhailova was supported by the Pasteur-Paris University (PPU) International Ph.D. Program. Amal Elfidha was supported by the ANRS. The study was supported with funds from the Institut Pasteur VALOEXPRESS Program. The ANRS pVISCONTI study was supported by ANRS and MSDAVENIR.

A.M., J.C.V.-C., A.D., V.M., and A.E. performed experiments; A.M., J.C.V.-C., A.D., V.M.,

S.V., and A.S.-C. analyzed the data; J.-L.P. and C.P. provided key reagents; J.-L.P. and A.S.-C. conceived the study; A.M., A.D., J.C.V.-C., and A.S.-C. designed the experiments; A.S.-C. supervised the study; A.M. and A.S.-C. drafted the article; and we all critically reviewed the manuscript.

A.M., A.D., J.-L.P., and A.S.-C. are listed as inventors in a patent application submitted by INSERM and Institut Pasteur partially based on the results described here. J.-L.P. is listed as inventor in a patent application related to the use of AAC-11 peptides in the treatment of cancer.

REFERENCES

1. Davey RT, Bhat N, Yoder C, Chun T-W, Metcalf JA, Dewar R, Natarajan V, Lempicki RA, Adelsberger JW, Miller KD, Kovacs JA, Polis MA, Walker RE, Falloon J, Masur H, Gee D, Baseler M, Dimitrov DS, Fauci AS, Lane HC. 1999. HIV-1, and T cell dynamics after interruption of highly active antiretroviral therapy (HAART) in patients with a history of sustained viral suppression. Proc Natl Acad Sci U S A 96:15109–15114. https://doi.org/10.1073/pnas.96.26.15109.
2. García F, Plana M, Vidal C, Cruceta A, O'Brien WA, Pantaleo G, Pumarola T, Gallart T, Miró JM, Gatell JM. 1999. Dynamics of viral load rebound and immunological changes after stopping effective antiretroviral therapy. AIDS 13:F79–F86. https://doi.org/10.1097/00002030-199907300-00002.
3. Harrigan PR, Whaley M, Montaner JS. 1999. Rate of HIV-1 RNA rebound upon stopping antiretroviral therapy. AIDS 13:F59–F62. https://doi.org/10.1097/00002030-199905280-00001.
4. Mikhailova A, Valle-Casuso JC, Sáez-Cirión A. 2018. Cellular determinants of HIV persistence on antiretroviral therapy, p 213–239. *In* Zhang L, Lewin SR (ed), HIV vaccines and cure: the path towards finding an effective cure and vaccine. Springer, Singapore.
5. Roederer M, Raju PA, Mitra DK, Herzenberg LA, Herzenberg LA. 1997. HIV does not replicate in naive CD4 T cells stimulated with CD3/CD28. J Clin Invest 99:1555–1564. https://doi.org/10.1172/JCI119318.
6. Schnittman SM, Lane HC, Greenhouse J, Justement JS, Baseler M, Fauci AS. 1990. Preferential infection of CD4+ memory T cells by human immunodeficiency virus type 1: evidence for a role in the selective T-cell functional defects observed in infected individuals. Proc Natl Acad Sci U S A 87:6058–6062. https://doi.org/10.1073/pnas.87.16.6058.
7. Valle-Casuso JC, Angin M, Volant S, Passaes C, Monceaux V, Mikhailova A, Bourdic K, Avettand-Fenoel V, Boufassa F, Sitbon M, Lambotte O, Thoulouze M-I, Müller-Trutwin M, Chomont N, Sáez-Cirión A. 2019. Cellular metabolism is a major determinant of HIV-1 reservoir seeding in CD4(+) T cells and offers an opportunity to tackle infection. Cell Metab 29:611–626 e615. https://doi.org/10.1016/j.cmet.2018.11.015.
8. Almeida L, Lochner M, Berod L, Sparwasser T. 2016. Metabolic pathways in T cell activation and lineage differentiation. Semin Immunol 28:514–524. https://doi.org/10.1016/j.smim.2016.10.009.
9. Hegedus A, Kavanagh Williamson M, Huthoff H. 2014. HIV-1 pathogenicity and virion production are dependent on the metabolic phenotype of activated CD4+ T cells. Retrovirology 11:98. https://doi.org/10.1186/s12977-014-0098-4.
10. Hollenbaugh JA, Munger J, Kim B. 2011. Metabolite profiles of human immunodeficiency virus infected CD4+ T cells and macrophages using LC-MS/MS analysis. Virology 415:153–159. https://doi.org/10.1016/j.virol.2011.04.007.
11. Heaton NS, Perera R, Berger KL, Khadka S, LaCount DJ, Kuhn RJ, Randall G. 2010. Dengue virus nonstructural protein 3 redistributes fatty acid synthase to sites of viral replication and increases cellular fatty acid synthesis. Proc Natl Acad Sci U S A 107:17345–17350. https://doi.org/10.1073/pnas.1010811107.
12. Manel N, Kim FJ, Kinet S, Taylor N, Sitbon M, Battini J-L. 2003. The ubiquitous glucose transporter GLUT-1 is a receptor for HTLV. Cell 115:449–459. https://doi.org/10.1016/S0092-8674(03)00881-X.
13. McArdle J, Moorman NJ, Munger J. 2012. HCMV targets the metabolic stress response through activation of AMPK whose activity is important for viral replication. PLoS Pathog 8:e1002502. https://doi.org/10.1371/journal.ppat.1002502.
14. Koci L, Chlebova K, Hyzdalova M, Hofmanova J, Jira M, Kysela P, Kozubik A, Kala Z, Krejci P. 2012. Apoptosis inhibitor 5 (API-5; AAC-11; FIF) is upregulated in human carcinomas in vivo. Oncol Lett 3:913–916.
15. Kim JW, Cho HS, Kim JH, Hur SY, Kim TE, Lee JM, Kim I-K, Namkoong SE. 2000. AAC-11 overexpression induces invasion and protects cervical cancer cells from apoptosis. Lab Invest 80:587–594. https://doi.org/10.1038/labinvest.3780063.
16. Cho H, Chung J-Y, Song K-H, Noh KH, Kim BW, Chung EJ, Ylaya K, Kim JH, Kim TW, Hewitt SM, Kim J-H. 2014. Apoptosis inhibitor-5 overexpression is associated with tumor progression and poor prognosis in patients with cervical cancer. BMC Cancer 14:545. https://doi.org/10.1186/1471-2407-14-545.
17. Sasaki H, Moriyama S, Yukiue H, Kobayashi Y, Nakashima Y, Kaji M, Fukai I, Kiriyama M, Yamakawa Y, Fujii Y. 2001. Expression of the antiapoptosis gene, AAC-11, as a prognosis marker in non-small cell lung cancer. Lung Cancer 34:53–57. https://doi.org/10.1016/S0169-5002(01)00213-6.
18. Wang Z, Liu H, Liu B, Ma W, Xue X, Chen J, Zhou Q. 2010. Gene expression levels of CSNK1A1 and AAC-11, but not NME1, in tumor tissues as prognostic factors in NSCLC patients. Med Sci Monit 16:CR357–CR364.
19. Han B-G, Kim KH, Lee SJ, Jeong K-C, Cho J-W, Noh KH, Kim TW, Kim S-J, Yoon H-J, Suh SW, Lee S, Lee BI. 2012. Helical repeat structure of apoptosis inhibitor 5 reveals protein-protein interaction modules. J Biol Chem 287:10727–10737. https://doi.org/10.1074/jbc.M111.317594.
20. Morris EJ, Michaud WA, Ji J-Y, Moon N-S, Rocco JW, Dyson NJ. 2006. Functional identification of Api5 as a suppressor of E2F-dependent apoptosis in vivo. PLoS Genet 2:e196. https://doi.org/10.1371/journal.pgen.0020196.
21. Rigou P, Piddubnyak V, Faye A, Rain J-C, Michel L, Calvo F, Poyet J-L. 2009. The antiapoptotic protein AAC–11 interacts with and regulates Acinus-mediated DNA fragmentation. EMBO J 28:1576–1588. https://doi.org/10.1038/emboj.2009.106.
22. Imre G, Berthelet J, Heering J, Kehrloesser S, Melzer IM, Lee BI, Thiede B, Dötsch V, Rajalingam K. 2017. Apoptosis inhibitor 5 is an endogenous inhibitor of caspase-2. EMBO Rep 18:733–744. https://doi.org/10.15252/embr.201643744.
23. Jagot-Lacoussiere L, Kotula E, Villoutreix BO, Bruzzoni-Giovanelli H, Poyet J-L. 2016. A cell-penetrating peptide targeting AAC-11 specifically induces cancer cells death. Cancer Res 76:5479–5490. https://doi.org/10.1158/0008-5472.CAN-16-0302.
24. Pasquereau-Kotula E, Habault J, Kroemer G, Poyet JL. 2018. The anticancer peptide RT53 induces immunogenic cell death. PLoS One 13:e0201220. https://doi.org/10.1371/journal.pone.0201220.
25. Habault J, Kaci A, Pasquereau-Kotula E, Fraser C, Chomienne C, Dombret H, Braun T, Pla M, Poyet JL. 2020. Prophylactic and therapeutic antileukemic effects induced by the AAC-11-derived peptide RT53. Oncoimmunology 9:1728871. https://doi.org/10.1080/2162402X.2020.1728871.
26. Akanji MA, Rotimi D, Adeyemi OS. 2019. Hypoxia-inducible factors as an alternative source of treatment strategy for cancer. Oxid Med Cell Longev 2019:8547846.
27. Diao L, Wang S, Sun Z. 2018. Long noncoding RNA GAPLINC promotes gastric cancer cell proliferation by acting as a molecular sponge of miR-378 to modulate MAPK1 expression. Onco Targets Ther 11:2797–2804. https://doi.org/10.2147/OTT.S165147.
28. Hottiger M, Gramatikoff K, Georgiev O, Chaponnier C, Schaffner W, Hubscher U. 1995. The large subunit of HIV-1 reverse transcriptase interacts with beta-actin. Nucleic Acids Res 23:736–741. [7535922]
29. Ishaq M, Lin BR, Bosche M, Zheng X, Yang J, Huang D, Lempicki RA, Aguilera-Gutierrez A, Natarajan V. 2011. LIM kinase 1-dependent cofilin 1 pathway and actin dynamics mediate nuclear retinoid receptor function in T lymphocytes. BMC Mol Biol 12:41. https://doi.org/10.1186/1471-2199-12-41.
30. Kalpana GV, Marmon S, Wang W, Crabtree GR, Goff SP. 1994. Binding and

stimulation of HIV-1 integrase by a human homolog of yeast transcription factor SNF5. Science 266:2002–2006. https://doi.org/10.1126/science.7801128.
31. Knudsen ES, Pruitt SC, Hershberger PA, Witkiewicz AK, Goodrich DW. 2019. Cell cycle and beyond: exploiting new RB1 controlled mechanisms for cancer therapy. Trends Cancer 5:308–324. https://doi.org/10.1016/j.trecan.2019.03.005.
32. Liu GY, Sabatini DM. 2020. mTOR at the nexus of nutrition, growth, ageing and disease. Nat Rev Mol Cell Biol 21:183–203. https://doi.org/10.1038/s41580-019-0199-y.
33. Liu X. 2019. SLC family transporters. Adv Exp Med Biol 1141:101–202. https://doi.org/10.1007/978-981-13-7647-4_3.
34. Naz H, Islam A, Waheed A, Sly WS, Ahmad F, Hassan I. 2013. Human beta-glucuronidase: structure, function, and application in enzyme replacement therapy. Rejuvenation Res 16:352–363. https://doi.org/10.1089/rej.2013.1407.
35. Paz S, Krainer AR, Caputi M. 2014. HIV-1 transcription is regulated by splicing factor SRSF1. Nucleic Acids Res 42:13812–13823. https://doi.org/10.1093/nar/gku1170.
36. Phuyal S, Farhan H. 2019. Multifaceted rho GTPase signaling at the endomembranes. Front Cell Dev Biol 7:127. https://doi.org/10.3389/fcell.2019.00127.
37. Seidler NW. 2013. GAPDH and intermediary metabolism. Adv Exp Med Biol 985:37–59. https://doi.org/10.1007/978-94-007-4716-6_2.
38. Stroud JC, Oltman A, Han A, Bates DL, Chen L. 2009. Structural basis of HIV-1 activation by NF-kappaB—a higher-order complex of p50:RelA bound to the HIV-1 LTR. J Mol Biol 393:98–112. https://doi.org/10.1016/j.jmb.2009.08.023.
39. Sun X, Kaufman PD. 2018. Ki-67: more than a proliferation marker. Chromosoma 127:175–186. https://doi.org/10.1007/s00412-018-0659-8.
40. Tahirov TH, Babayeva ND, Varzavand K, Cooper JJ, Sedore SC, Price DH. 2010. Crystal structure of HIV-1 Tat complexed with human P-TEFb. Nature 465:747–751. https://doi.org/10.1038/nature09131.
41. Wu Y, Zhou X, Barnes CO, DeLucia M, Cohen AE, Gronenborn AM, Ahn J, Calero G. 2016. The DDB1-DCAF1-Vpr-UNG2 crystal structure reveals how HIV-1 Vpr steers human UNG2 toward destruction. Nat Struct Mol Biol 23:933–940. https://doi.org/10.1038/nsmb.3284.
42. Allouch A, David A, Amie SM, Lahouassa H, Chartier L, Margottin-Goguet F, Barré-Sinoussi F, Kim B, Sáez-Cirión A, Pancino G. 2013. p21-mediated RNR2 repression restricts HIV-1 replication in macrophages by inhibiting dNTP biosynthesis pathway. Proc Natl Acad Sci U S A 110:E3997–E4006. https://doi.org/10.1073/pnas.1306719110.
43. Derossi D, Chassaing G, Prochiantz A. 1998. Trojan peptides: the penetratin system for intracellular delivery. Trends Cell Biol 8:84–87. https://doi.org/10.1016/S0962-8924(98)80017-2.
44. Sáez-Cirión A, Hamimi C, Bergamaschi A, David A, Versmisse P, Mélard A, Boufassa F, Barré-Sinoussi F, Lambotte O, Rouzioux C, Pancino G, ANRS CO18 Cohort. 2011. Restriction of HIV-1 replication in macrophages and CD4+ T cells from HIV controllers. Blood 118:955–964. https://doi.org/10.1182/blood-2010-12-327106.
45. Elliott JI, Sardini A, Cooper JC, Alexander DR, Davanture S, Chimini G, Higgins CF. 2006. Phosphatidylserine exposure in B lymphocytes: a role for lipid packing. Blood 108:1611–1617. https://doi.org/10.1182/blood-2005-11-012328.
46. Bortner CD, Hughes FM, Cidlowski JA. 1997. A primary role for K+ and Na+ efflux in the activation of apoptosis. J Biol Chem 272:32436–32442. https://doi.org/10.1074/jbc.272.51.32436.
47. McCarthy JV, Cotter TG. 1997. Cell shrinkage and apoptosis: a role for potassium and sodium ion efflux. Cell Death Differ 4:756–770. https://doi.org/10.1038/sj.cdd.4400296.
48. Yu SP. 2003. Regulation and critical role of potassium homeostasis in apoptosis. Prog Neurobiol 70:363–386. https://doi.org/10.1016/S0301-0082(03)00090-X.
49. Thompson GJ, Langlais C, Cain K, Conley EC, Cohen GM. 2001. Elevated extracellular [K+] inhibits death-receptor- and chemical-mediated apoptosis prior to caspase activation and cytochrome c release. Biochem J 357:137–145. https://doi.org/10.1042/bj3570137.
50. Tewari M, Yu M, Ross B, Dean C, Giordano A, Rubin R. 1997. AAC-11, a novel cDNA that inhibits apoptosis after growth factor withdrawal. Cancer Res 57:4063–4069. [9307294]
51. Galluzzi L, Kepp O, Vander Heiden MG, Kroemer G. 2013. Metabolic targets for cancer therapy. Nat Rev Drug Discov 12:829–846. https://doi.org/10.1038/nrd4145.
52. Green DR, Galluzzi L, Kroemer G. 2014. Cell biology. Metabolic control of cell death. Science 345:1250256. https://doi.org/10.1126/science.1250256.
53. Imre G, Heering J, Takeda A-N, Husmann M, Thiede B, zu Heringdorf DM, Green DR, van der Goot FG, Sinha B, Dötsch V, Rajalingam K. 2012. Caspase-2 is an initiator caspase responsible for pore-forming toxin-mediated apoptosis. EMBO J 31:2615–2628. https://doi.org/10.1038/emboj.2012.93.
54. Sorbara LR, Maldarelli F, Chamoun G, Schilling B, Chokekijcahi S, Staudt L, Mitsuya H, Simpson IA, Zeichner SL. 1996. Human immunodeficiency virus type 1 infection of H9 cells induces increased glucose transporter expression. J Virol 70:7275–7279. https://doi.org/10.1128/JVI.70.10.7275-7279.1996.
55. Campbell GR, To RK, Spector SA. 2019. TREM-1 protects HIV-1-infected macrophages from apoptosis through maintenance of mitochondrial function. mBio 10:e02638-19. https://doi.org/10.1128/mBio.02638-19.
56. Huang SH, Ren Y, Thomas AS, Chan D, Mueller S, Ward AR, Patel S, Bollard CM, Cruz CR, Karandish S, Truong R, Macedo AB, Bosque A, Kovacs C, Benko E, Piechocka-Trocha A, Wong H, Jeng E, Nixon DF, Ho YC, Siliciano RF, Walker BD, Jones RB. 2018. Latent HIV reservoirs exhibit inherent resistance to elimination by CD8+ T cells. J Clin Invest 128:876–889. https://doi.org/10.1172/JCI97555.
57. Kuo HH, Ahmad R, Lee GQ, Gao C, Chen HR, Ouyang Z, Szucs MJ, Kim D, Tsibris A, Chun TW, Battivelli E, Verdin E, Rosenberg ES, Carr SA, Yu XG, Lichterfeld M. 2018. Anti-apoptotic Protein BIRC5 maintains survival of HIV-1-infected CD4(+) T cells. Immunity 48:1183–1194 e1185. https://doi.org/10.1016/j.immuni.2018.04.004.
58. Huddleston CA, Weinberg AD, Parker DC. 2006. OX40 (CD134) engagement drives differentiation of CD4+ T cells to effector cells. Eur J Immunol 36:1093–1103. https://doi.org/10.1002/eji.200535637.
59. Redmond WL, Ruby CE, Weinberg AD. 2009. The role of OX40-mediated co-stimulation in T-cell activation and survival. Crit Rev Immunol 29:187–201. https://doi.org/10.1615/CritRevImmunol.v29.i3.10.
60. Pacella I, Procaccini C, Focaccetti C, Miacci S, Timperi E, Faicchia D, Severa M, Rizzo F, Coccia EM, Bonacina F, Mitro N, Norata GD, Rossetti G, Ranzani V, Pagani M, Giorda E, Wei Y, Matarese G, Barnaba V, Piconese S. 2018. Fatty acid metabolism complements glycolysis in the selective regulatory T cell expansion during tumor growth. Proc Natl Acad Sci U S A 115:E6546–E6555. https://doi.org/10.1073/pnas.1720113115.
61. Valle-Casuso JC, Allouch A, David A, Lenzi GM, Studdard L, Barré-Sinoussi F, Müller-Trutwin M, Kim B, Pancino G, Sáez-Cirión A. 2017. p21 restricts HIV-1 in monocyte-derived dendritic cells through the reduction of deoxynucleoside triphosphate biosynthesis and regulation of SAMHD1 antiviral activity. J Virol 91:e01324-17.
62. Sallusto F, Lanzavecchia A, Araki K, Ahmed R. 2010. From vaccines to memory and back. Immunity 33:451–463. https://doi.org/10.1016/j.immuni.2010.10.008.
63. Salgado M, Kwon M, Galvez C, Badiola J, Nijhuis M, Bandera A, Balsalobre P, Miralles P, Buno I, Martinez-Laperche C, Vilaplana C, Jurado M, Clotet B, Wensing A, Martinez-Picado J, Diez-Martin JL, for the IciStem Consortium. 2018. Mechanisms that contribute to a profound reduction of the HIV-1 reservoir after allogeneic stem cell transplant. Ann Intern Med 169:674–683. https://doi.org/10.7326/M18-0759.
64. David A, Sáez-Cirión A, Versmisse P, Malbec O, Iannascoli B, Herschke F, Lucas M, Barré-Sinoussi F, Mouscadet J-F, Daëron M, Pancino G. 2006. The engagement of activating FcγRs inhibits primate lentivirus replication in human macrophages. J Immunol 177:6291–6300. https://doi.org/10.4049/jimmunol.177.9.6291.